Doc# 220244

UCRL-JC-108830
PREPRINT

CARBON AEROGELS AND XEROGELS

Richard W. Pekala
Cynthia T. Alviso

This paper was prepared for submittal to
Materials Research Society
1992 Spring Meeting
San Francisco, CA
April 27-May 1, 1992

April 1992

Lawrence Livermore National Laboratory

This is a preprint of a paper intended for publication in a journal or proceedings. Since changes may be made before publication, this preprint is made available with the understanding that it will not be cited or reproduced without the permission of the author.

DISCLAIMER

This document was prepared as an account of work sponsored by an agency of the United States Government. Neither the United States Government nor the University of California nor any of their employees, makes any warranty, express or implied, or assumes any legal liability or responsibility for the accuracy, completeness, or usefulness of any information, apparatus, product, or process disclosed, or represents that its use would not infringe privately owned rights. Reference herein to any specific commercial products, process, or service by trade name, trademark, manufacturer, or otherwise, does not necessarily constitute or imply its endorsement recommendation, or favoring of the United States Government or the University of California. The views and opinions of authors expressed herein do not necessarily state or reflect those of the United States Government or the University of California, and shall not be used for advertising or product endorsement purposes.

CARBON AEROGELS AND XEROGELS

Richard W. Pekala and Cynthia T. Alviso
Chemistry & Materials Science Department
Lawrence Livermore National Laboratory
Livermore, CA 94550

ABSTRACT

The aqueous polycondensation of resorcinol with formaldehyde proceeds through a sol-gel transition and results in the formation of highly crosslinked, transparent gels. If the solvent is simply evaporated from the pores of these gels, large capillary forces are exerted and a collapsed structure known as a *xerogel* is formed. In order to preserve the gel skeleton and minimize shrinkage, the aforementioned solvent or its substitute must be removed under supercritical conditions. The microporous material that results from this operation is known as an *aerogel.*

Because resorcinol-formaldehyde aerogels and xerogels consist of a highly crosslinked aromatic polymer, they can be pyrolyzed in an inert atmosphere to form vitreous carbon monoliths. The resultant porous materials are black in color and no longer transparent, yet they retain the ultrafine cell size (< 50 nm), high surface area (600-800 m^2/g), and the interconnected particle morphology of their organic precursors. The thermal, acoustic, mechanical, and electrical properties of carbon aerogels/xerogels primarily depend upon polymerization conditions and pyrolysis temperature. In this paper, the chemistry-structure-property relationships of these unique materials will be discussed in detail.

INTRODUCTION

A number of methods are used to generate low density carbon foams: (1) phenolic microballoons are stabilized with an appropriate binder and pyrolyzed to form syntactic carbon foams, (2) the partial oxidation and pyrolysis of phase-separated polyacrylonitrile foams results in microcellular carbon foams, (3) reticulated vitreous carbon (RVC) foams are produced by pyrolyzing an open-cell polyurethane foam that has been infused with a reactive monomer such as furfuryl alcohol, and (4) replica carbon foams result from the pyrolysis of a phenolic resin within a sacrificial substrate that is subsequently removed [1-4]. In each of these cases, processing parameters control the morphology, density, and cell size distribution of the final foam. In general, it is difficult to achieve carbon foams that have *both* low density (< 0.1 g/cc) and small cell size (< 25 μ).

In the past 5 years, our research has focused on sol-gel polymerizations that lead to organic-based aerogels that can be subsequently pyrolyzed into carbon aerogels. Aerogels are a special class of open-cell foams that have high porosity, ultrafine cell/pore sizes (< 50 nm), high surface area (400-1000 m^2/g), and a solid matrix composed of interconnected colloidal-like particles or fibrous chains with characteristic diameters of 10 nm. The densified version of an aerogel is known as a xerogel.

Traditional sol-gel polymerizations have involved the hydrolysis and condensation of metal alkoxides (e.g. tetramethoxy silane, tantalum ethoxide) to form xerogels that are sintered into full density glasses or ceramics [5-8]. This approach is particularly attractive because materials with superior homogeneity and new compositions can be achieved. Other investigators have preserved the delicate gel structure by extracting the solvent within the pores under supercritical conditions to form aerogels. Silica aerogels have been widely studied and are finding promising applications as thermal insulators, acoustic impedance matching devices, and catalyst supports [9-11].

Several organic reactions that proceed through a sol-gel transition have been identified [12-15]. The most-studied reaction involves the aqueous polycondensation of resorcinol (1,3 dihydroxybenzene) with formaldehyde, although other dihydroxy and trihydroxy benzene compounds can be used. The resultant gels are either evaporatively dried to form xerogels or supercritically dried to form aerogels. The resorcinol-formaldehyde (RF) aerogels and xerogels can be further processed at high temperatures in an inert atmosphere to form vitreous carbon monoliths. The chemistry-structure-property relationships of carbon aerogels and xerogels are outlined in this paper.

EXPERIMENTAL

The preparation of RF gels involved mixing resorcinol powder (Aldrich; 98%) and formaldehyde (Aldrich; 37.5%; methanol stabilized) in a 1:2 molar ratio. Deionized and

distilled water was added as the diluent and sodium carbonate as the base catalyst. After stirring to form a homogeneous solution, the mixture was poured into 25 mm diameter x 80 mm long glass vials, sealed, and cured at elevated temperature. For solutions containing ≤ 10 w/v % reactants, the sol-gel polymerization was conducted for 7 days at 85-95 °C. At higher reactant concentrations, the solutions were cured for 1 day at room temperature followed by 1 day at 50 °C and 3 days at 85-95 °C. The latter procedure prevented the formation of trapped air bubbles within the gel due to the large exotherm at elevated temperatures. [Resorcinol] / [Catalyst] (R/C) ratios of 50-300 were used to form transparent gels, while opaque gels were formed at R/C values ≥ 400.

Upon completion of the cure cycle, the caps were removed from some glass containers and the water allowed to evaporate, resulting in the formation of an RF xerogel. In other cases, the RF gels were removed from their glass containers and placed in an agitated acetone bath. The first acetone wash contained a small amount of trifluoroacetic acid (~0.1%) to promote further crosslinking of hydroxymethyl groups within the gel. Two additional washes with fresh acetone were carried out to ensure complete replacement of the water which originally occupied the pores of the RF gel.

The acetone-filled gels were then placed in a jacketed pressure vessel (Polaron®, Watford, England) which was subsequently filled with liquid carbon dioxide at 10 °C. The RF gels were exchanged with fresh carbon dioxide until the acetone was completely flushed from the system. At no time was the liquid CO_2 level allowed to drop below the top of the RF gels. The pressure vessel was taken above the critical point of carbon dioxide (T_c= 31°C; P_c= 7.4 MPa) and held at ~45 °C and ~11 MPa for a minimum of 4 hours. While maintaining the temperature, the pressure was slowly bled from the vessel overnight. At atmospheric pressure, the aerogels were removed from the vessel and evaluated.

RF aerogels and xerogels are dark red in color, but they do transmit light. Pyrolysis of these materials was performed in a 3-zone Lindberg furnace (Model #54657-S) under nitrogen flow with the following ramp cycle: 22 °C → 250 °C in 2 hrs., held at 250 °C for 4 hrs., 250 °C → 1050 °C in 9.5 hrs., and held at 1050 °C for 4 hrs. The furnace was then allowed to cool under its own thermal mass back to room temperature in ~16 hrs. The carbon aerogels and xerogels are opaque and black in color. Pyrolysis leads to volumetric shrinkages of 65-75 % with an accompanying mass loss of ~50 %.

The modulus and strength of organic aerogels were measured in uniaxial compression with an Instron machine (model #1125) [16]. Surface areas and pore size distributions were determined from nitrogen and argon adsorption analysis [17]. Scanning electron microscopy (Hitachi S-800) and transmission electron microscopy (Jeol 200 CX) were used to examine the morphologies of organic aerogels. Small angle x-ray scattering data were obtained with the 10 meter point collimated instrument at Oak Ridge National Laboratory. Thermal conductivity measurements were performed using a hot-wire

technique [18]. Electrical resistivity data were collected as described previously [19].

RESULTS AND DISCUSSION

The aqueous, polycondensation of resorcinol with formaldehyde proceeds through a sol-gel transition as outlined in Figure 1. In this polymerization, resorcinol is a trifunctional monomer capable of adding formaldehyde in the 2-,4-, and/or 6- ring positions. This monomer along with other di- and tri-hydroxy benzene compounds is particularly reactive because of the (1) electron-donating and (2) *ortho-*, *para-* directing effects of the attached hydroxyl groups. The substituted resorcinol rings condense with each other to form nanometer-sized clusters in solution. The size of the clusters is regulated by the catalyst concentration (i.e. sodium carbonate) in the resorcinol-formaldehyde (RF) mixture. Eventually, the clusters crosslink through their surface functional groups (e.g. $-CH_2OH$) to form a gel. RF gels, aerogels, and xerogels are dark red in color as a result of oxidation products formed during the polymerization. After pyrolysis, these porous materials turn black.

The [Resorcinol]/[Catalyst] ratio is the dominant factor which affects the density, particle size, surface area, and mechanical properties of both RF and carbon aerogels [12-13,16,20-21]. TEM shows that these materials are composed of interconnected colloidal-like particles derived from the clusters formed during the sol-gel polymerization. Under high catalyst condititions (i.e. R/C=50), RF aerogels have interconnected particles with diameters of 3-5 nm that are tightly fused together, giving the aerogel a fibrous appearance. Under low catalyst conditions (i.e. R/C=200), RF aerogels have interconnected particles with diameters of 11-14 nm that are loosely bonded to each other. While the particle size, surface area, and interconnections between particles are modified upon pyrolysis, carbon aerogels share a similar 'string-of-pearls' morphology to their RF precursors. TEMs of RF and carbon aerogels synthesized at R/C= 50 and R/C= 200 are shown in Figure 2. This same interconnected particle morphology is observed in the corresponding xerogels.

In order to more fully probe the aerogel nanostructure, small angle x-ray scattering (SAXS) data were collected for a series of carbon aerogels with R/C values of 50-300. Disordered materials such as aerogels often display "dilation symmetry", and small angle scattering is a convenient method for determining the fractal dimensions (D_m,D_s) of a porous material. For fractal structures, the SAXS intensity I(q) shows a power law dependence on the scattering vector q such that [22]:

Mass Fractal	$I(q) \sim q^{-D_m}$	$1 < D_m < 3$	[1]
Surface Fractal	$I(q) \sim q^{-(6-D_s)}$	$3 < 6-D_s < 4$	[2]

The q-range over which these relationships hold is limited on the low end by a value q_c, corresponding to the reciprocal of the structural correlation length, ξ. The maximum value q_u is determined by $1/\beta$, where β is the average radius of the fundamental structural units that build up the fractal structure.

Figure 3 shows a log-log plot of SAXS intensity versus scattering vector, q, for carbon aerogels at various R/C ratios. These curves have been displaced along the vertical axis for clarity. For each curve, a constant intensity is observed at small values of q, consistent with a uniform long-range structure --- i.e. the aerogels are homogeneous at length scales greater than 50 nm.

In a porous material, the position of the break in I(q) in the Guinier regime provides a measure of the correlation length, ξ, which approximates the mean pore radius [23]. The mean pore size depends upon both the density and R/C ratio of the carbon aerogels. In general, the mean pore radius of carbon aerogels as determined by SAXS is less than 10 nm. The ultrafine pore sizes of these aerogels are responsible for their unique thermal, acoustic, and electrical properties.

In the Porod regime (intermediate q values), the SAXS curves continue to decrease monotonically. In this regime, dimensions that are larger than chemical bond distances but smaller than the mean pore size are being probed. For fractal materials, a power law relationship between I(q) and q is expected. It is clear that carbon aerogels do not exhibit this behavior over any extended range of q, and thus, are <u>not</u> mass fractals. This result contrasts with silica aerogels that have been shown to be mass fractals over more than a decade of q space. At high q values, the SAXS curves reach a limiting slope of -4, indicative of a smooth interface at the surface of the interconnected particles.

The pore size distribution of carbon aerogels can also be obtained from gas adsorption analyses [17]. Two pore size ranges can be differentiated in carbon aerogels: (1) micropores with diameters less than 2 nm which reside within the individual carbon particles and (2) mesopores which span the distance between the interconnected 'strings-of-pearls'. A series of carbon aerogels with different bulk densities were synthesized at a fixed R/C= 200 ratio, ensuring that the interconnected particle size and BET surface area (647 ± 49 m^2/g) were approximately the same in all specimens. Figure 4 shows the dependence of the average mesopore size upon the aerogel density. As expected, the mesopore size decreases with aerogel density, and the data display a power-law fit with a scaling exponent of -1.05.

The ultrafine cell/pore size and low density of carbon aerogels is responsible for their low thermal conductivity as compared to full density glassy carbon. The total conductivity (λ_t) of air filled monolithic aerogels is

$$\lambda_t = \lambda_r + \lambda_s + \lambda_g \qquad [3]$$

where λ_r is the radiative contribution, λ_g is the gaseous conductivity, and λ_s is the solid conductivity. The radiative component of the total conductivity is practically independent of aerogel density, while the solid conductivity increases in a monotonic fashion. The gaseous conductivity shows an inverse relationship with aerogel density and becomes a major factor at low densities where the cell/pore size increases . In Figure 5, the thermal conductivity of carbon aerogels is plotted as a function of aerogel density. The thermal conductivity of carbon aerogels is much higher than silica or RF aerogels due to the higher solid conductivity of the carbon matrix (~4.1 W/m-K). Nevertheless, some of these materials have thermal conductivities which are a factor of 100 less than fully dense glassy carbon [24]. Unlike silica and RF aerogels, a minimum has not yet been observed in the thermal conductivity curve of carbon aerogels. Nevertheless, we believe such an observation will be made when carbon aerogels of even lower densities are tested.

The interconnections between carbon particles are particularly important to the mechanical properties of carbon aerogels [16,20]. Figure 6 shows the compressive modulus of carbon aerogels as a function of density and R/C ratio. As expected, the modulus increases as a function of bulk density. The linear log-log plot in each case demonstrates a power-law density dependence that has been observed in many other low density materials [25]. This relationship is expressed as

$$E = cd^n \qquad [4]$$

where d is the bulk density, c is a constant (prefactor), and n is a non-integer exponent that usually ranges from 2-4. For highly regular open-cell foams, the exponent usually falls very close to 2.0 while ideal closed-cell foams give an exponent of 3.0. Foams with irregular, fractal type morphologies generally have a value that exceeds 3.0.

In the case of carbon aerogels, the above exponent equals 2.7 ± 0.2. Although the scaling exponents are the same for all formulations, the prefactors scale inversely with the R/C ratio. As the R/C ratio and the interconnected particle size decrease, the modulus increases due to an apparent improvement in the particle interconnectivity. This same trend holds for the compressive strength of carbon aerogels, but the scaling exponent is 2.4 ± 0.3. Carbon aerogels are superior in both stiffness and strength when compared to their RF precursors at equivalent densities and R/C ratios. In general, pyrolysis leads to a 10-25 fold increase in these physical properties.

Sound propagation (0.01-5 MHz) within carbon aerogels and xerogels also shows a power-law dependence upon bulk density. The scaling exponent is 0.82 ± 0.07 over a density range of 0.05-1.3 g/cc. At 0.1 g/cc, carbon aerogels display a longitudinal sound velocity of 500 m/s. One of the most striking features of carbon aerogels with densities less than 0.08 g/cc is the decrease of sound velocity upon uniaxial compression (1-3 %

strain). This same phenomenon has been observed in silica and RF aerogels, and it has been explained by a "knee model" for the internal structure [26].

A major advantage of pyrolysis is the formation of an electrically conductive aerogel. The low resistivity of these porous materials coupled with their high surface areas is being exploited in double layer capacitor applications. Figure 7 shows the temperature dependence of the resistivity for carbon aerogels synthesized at R/C=200. The data show that the resistivity falls as the density increases, as would be expected for a percolating network. Of particular interest is the sharp increase in resistivity at low temperature (below 30 K) for all samples. The effect is most striking for the least dense sample [27].

To obtain further information on the conduction mechanism, the low temperature data were plotted as log ρ vs. $1/T^n$, where ρ is the resistivity and n= 1/4, 1/3, 1/2, or 1. The least dense sample was found to fit a log ρ vs. 1/T plot quite well, while the higher density samples showed a log ρ vs. $1/T^{1/2}$ dependence, or perhaps even a $1/T^{1/3}$ dependence for the most dense sample. These transport measurements show that the temperature dependence of the resistivity is a sensitive characterization probe for the aerogels. At room temperature, the variation of resistivity for the highest and lowest density samples is about a factor of 30. At low temperatures, the difference is several orders of magnitude. Of interest also is the difference in the low temperature conduction mechanism for the least dense aerogel which appears to be a simple activation process, perhaps associated with hopping from one particle to another. For the denser aerogels, the functional form is consistent either with a charge-energy-limited tunneling conduction (CELTC) mechanism or with 1D variable-range hopping. An expanded discussion of these mechanisms and other transport properties will appear in a future publication [27].

Recently, we have begun to probe the carbon structure within the interconnected particles. Gas adsorption analysis has shown that these particles contain numerous micropores (< 2 nm). We also expected that some closed pores would exist in these particles, as is the case with most glassy carbons. Helium pycnometry reveals a skeletal density of 2.06 ± 0.06 g/cc for carbon aerogels synthesized at R/C= 200. This value is much higher than that of typical glassy carbons (1.46-1.50 g/cc) but lower than that of graphite (2.25 g/cc), suggesting that there are relatively few closed pores within the carbon particles. In a separate water immersion test, the skeletal density of carbon aerogels was determined to be 1.6 g/cc. These data imply that the microporosity of the individual carbon particles is not easily accessible.

Figure 8 shows Raman spectra for carbon aerogels of different densities synthesized at R/C= 200. The spectra are almost identical for each of the aerogels; however, a small reduction in linewidth is seen with increasing bulk density. The ratios of the integrated intensities of the disorder-induced line to that of the Raman-active line (I_{1360}/I_{1580}) were computed and the results were used to calculate the in-plane microcrystallite size (L_a) according to Knight's formula [28]. The in-plane microcrystallite size of 2.5-3.0 nm was

the same for all samples and much smaller than the interconnected particle size. Raman spectra for carbon aerogels synthesized at R/C= 50 and R/C= 300 showed microcrystallite sizes within the above range. These data suggest a model in which there is an interwoven mesh of microcrystallites within the individual carbon particles. High resolution TEM also provides evidence for such a structure.

CONCLUSIONS

Carbon aerogels and xerogels are novel forms of porous carbon available in densities ranging from 0.04-1.3 g/cc. These materials have ultrafine cell/pore sizes (< 50 nm), high surface areas (600-800 m^2/g), and a 'string-of-pearls' morphology. The individual carbon particles contain an interwoven mesh of microcrystalline platelets with tiny micropores (~0.6 nm). This nanostructure is responsible for the unique thermal, acoustic, electrical, and mechanical properties of carbon aerogels/xerogels.

ACKNOWLEDGMENTS

This work was performed under the auspices of the U.S. Department of Energy by Lawrence Livermore National Laboratory under contract #W-7405-ENG-48. The author would like to thank the following individuals for their technical contributions to this research project: Dr. James LeMay (mechanical properties), Suzy Hulsey (gas adsorption analyses), Dr. Dale Schaefer at SNLA (small angle x-ray scattering), Professor Jochen Fricke and Xianping Lu at the University of Wurzburg (thermal conductivity), and Professor Mildred Dresselhaus and Alex Fung at MIT (Raman spectra; low temperature resistivity).

REFERENCES

[1] S.T. Benton and C.R. Schmitt, Carbon, 10, 185 (1972).
[2] R.W. Pekala and R.W. Hopper, J. Mat. Sci., 22, 1840 (1987).
[3] A.P. Sylwester, J.H. Aubert, P.B. Rand, C. Arnold Jr., and R.L. Clough, Am. Chem. Soc. PMSE Preprint, 57, 113 (1987).
[4] H.C. Geer, in Encyclopedia of Polymer Science and Technology, edited by H.F. Mark, N.G. Gaylord, and N.M. Bikales (Interscience, New York, 1970), p. 102.
[5] L.L. Hench and J.K. West, Chem. Rev., 90, 33 (1990).
[6] D.R. Ulrich, Chem. & Eng. News, 68(1), 28 (1990).
[7] S.J. Teichner, G.A. Nicolaon, M.A. Vicarini, G.E.E. Gardes, Adv. Coll. Interf. Sci., 5, 245 (1976).
[8] C.J. Brinker and G.W. Scherer, Sol-Gel Science, (Academic Press, New York,

1990).
[9] J. Fricke, Sci. Am., 258(5), 92 (1988).
[10] Aerogels, edited by J. Fricke, (Springer-Verlag, New York, 1986).
[11] L.W. Hrubesh, T.M. Tillotson, and J.F. Poco, in Better Ceramics Through Chemistry IV, edited by C.J. Brinker, D.E. Clark, D.R. Ulrich, and B.J. Zelinski, (Mat. Res. Soc. Proc. 180, Pittsburgh, PA, 1990), pp. 315-319.
[12] R.W. Pekala, J. Mat. Sci., 24, 3221 (1989).
[13] R.W. Pekala and F.M. Kong, Polym. Prpts., 30(1), 221 (1989).
[14] C.T. Alviso and R.W. Pekala, Polym. Prpts., 32(3), 242 (1991).
[15] R.W. Pekala and C.T. Alviso, in Better Ceramics Through Chemistry IV, edited by C.J. Brinker, D.E. Clark, D.R. Ulrich, and B.J. Zelinski, (Mat. Res. Soc. Proc. 180, Pittsburgh, PA, 1990), pp. 791-795.
[16] R.W. Pekala, C.T. Alviso, and J.D. LeMay, J. Non-Cryst. Solids, 125, 67 (1990).
[17] S.S. Hulsey, C.T. Alviso, F.M. Kong, and R.W. Pekala, in this MRS proceedings.
[18] X. Lu, M.C. Arduini-Schuster, J. Kuhn, O. Nilsson, J. Frickes, and R.W. Pekala, Science, 255, 971 (1992).
[19] S.L. diVittorio, M.S. Dresselhaus, M. Endo, J-P. Issi, L. Piraux, and V. Bayot, J. Mat. Res., 6(4), 778 (1991).
[20] J.D. LeMay, R.W. Hopper, L.W. Hrubesh, and R.W. Pekala, MRS Bulletin, 15(12), 19 (1990).
[21] R.W. Pekala and F.M. Kong, J. de Physique Coll. Suppl., 50(4), C4-33 (1989).
[22] K.D. Keefer and D.W. Schaefer, Phys. Rev. Lett., 56(20), 2199 (1986).
[23] D.W. Schaefer, J.P. Wilcoxon, K.D. Keefer, B.C. Bunker, R.K. Pearson, I.M. Thomas, and D.E. Miller, in Physics and Chemistry of Porous Media II, edited by J.R. Banavar, J. Koplik, and K.W. Winkler, (AIP Conf. Proc. 154, New York, 1986), pp. 63-80.
[24] G.M. Jenkins and K. Kawamura, Polymeric Carbons - Carbon Fibre, Glass and Char, (Cambridge Univ. Press, New York, 1976) p. 84.
[25] L.J. Gibson and M.F. Ashby, Proc. Royal Soc. Long., 382(A), 43 (1982).
[26] J. Gross, J. Fricke, R.W. Pekala, and L.W. Hrubesh, Phys. Rev. B, in press.
[27] A.W. P. Fung and M.S. Dresselhaus (private communication).
[28] D.S. Knight and W.B. White, J. Mat. Res., 4, 385 (1989).

FIGURE CAPTIONS

Figure 1. The sol-gel polymerization of resorcinol with formaldehyde.

Figure 2. Transmission electron micrographs of RF and carbon aerogels synthesized at R/C= 50 and R/C= 200.

Figure 3. Small angle x-ray scattering curves for carbon aerogels synthesized at various R/C ratios: (a) 50, (b) 100, (c) 150, (d) 200, and (e) 300. Sample densities are 0.207, 0.136, 0.099, 0.103, and 0.085 g/cc, respectively.

Figure 4. A plot of average mesopore size vs. aerogel density.

Figure 5. The thermal conductivity of carbon aerogels as a function of density.

Figure 6. A log-log plot of compressive modulus vs. density for carbon aerogels synthesized at different R/C ratios.

Figure 7. The resistivity of carbon aerogels as a function of temperature and density. All samples were prepared at R/C= 200 and were pyrolyzed at 1050 °C.

Figure 8. The Raman spectra of carbon aerogels having different densities. All samples were prepared at R/C= 200.

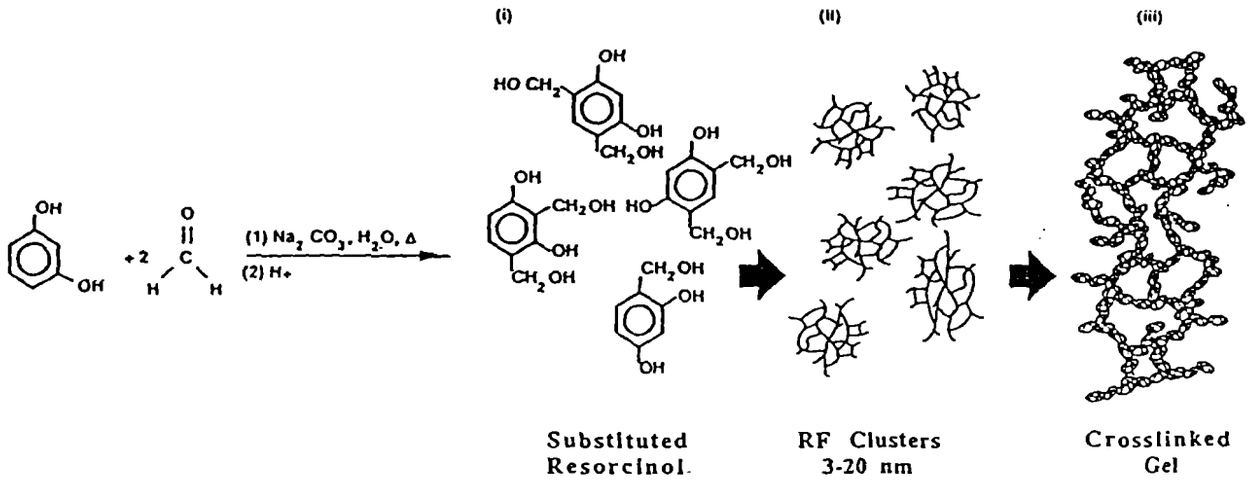
(i)
(ii)
(iii)
(1) Na2 CO3, H2O, Δ
(2) H+
Substituted Resorcinol
RF Clusters 3-20 nm
Crosslinked Gel

Fig. 1

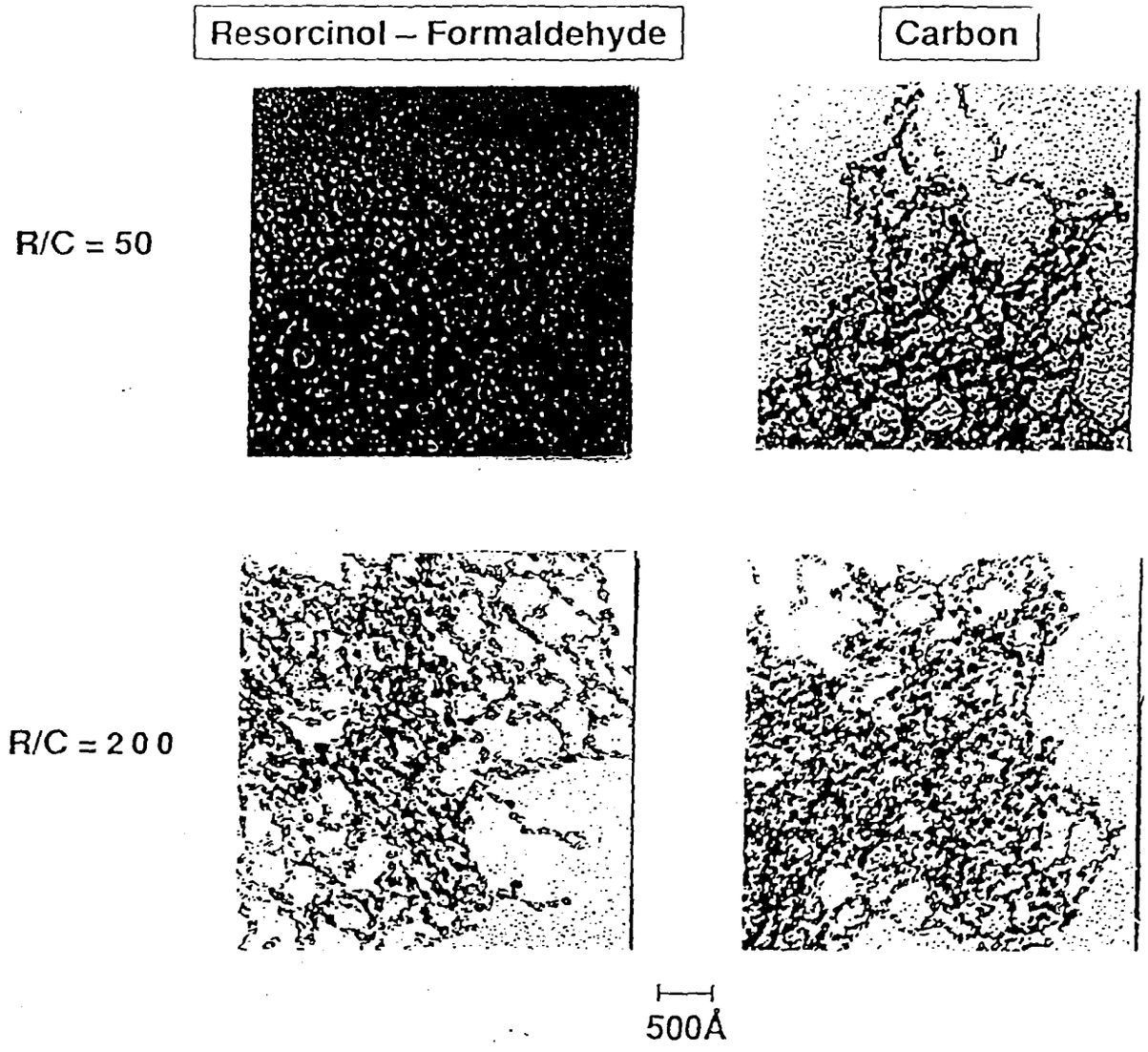

Fig. 2

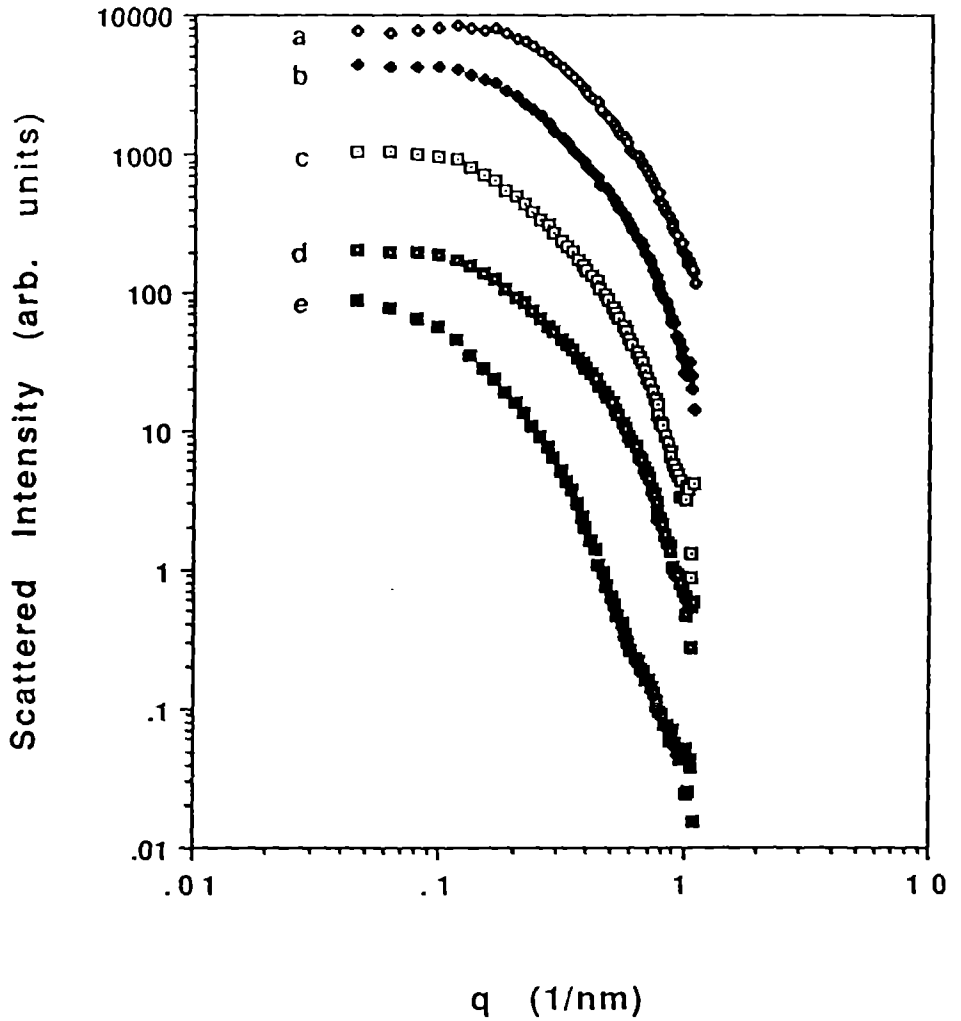
10000
1000
100
10
1
.1
.01
a
b
c
d
e
Scattered Intensity (arb. units)
.01
.1
1
10
q (1/nm)

Fig. 3

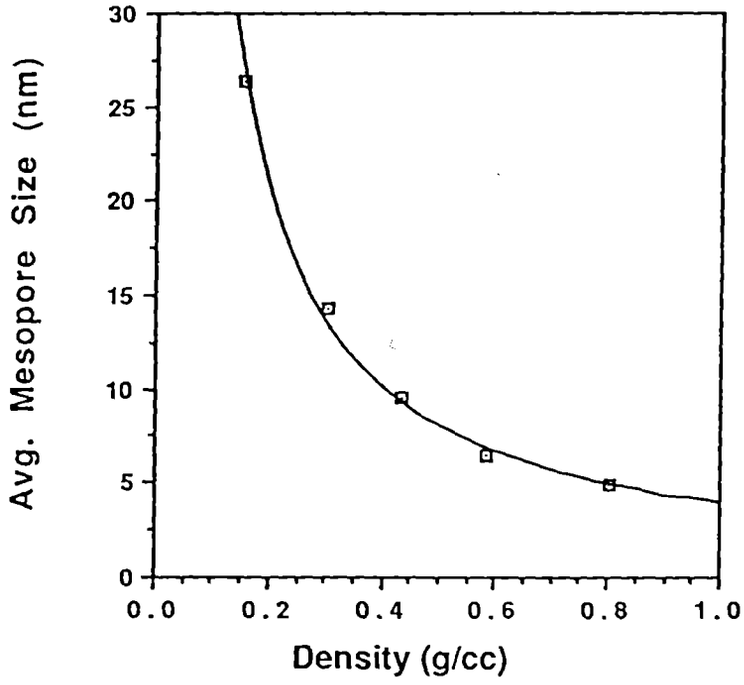
Avg. Mesopore Size (nm)
30
25
20
15
10
5
0
0.0
0.2
0.4
0.6
0.8
1.0
Density (g/cc)

Fig. 4

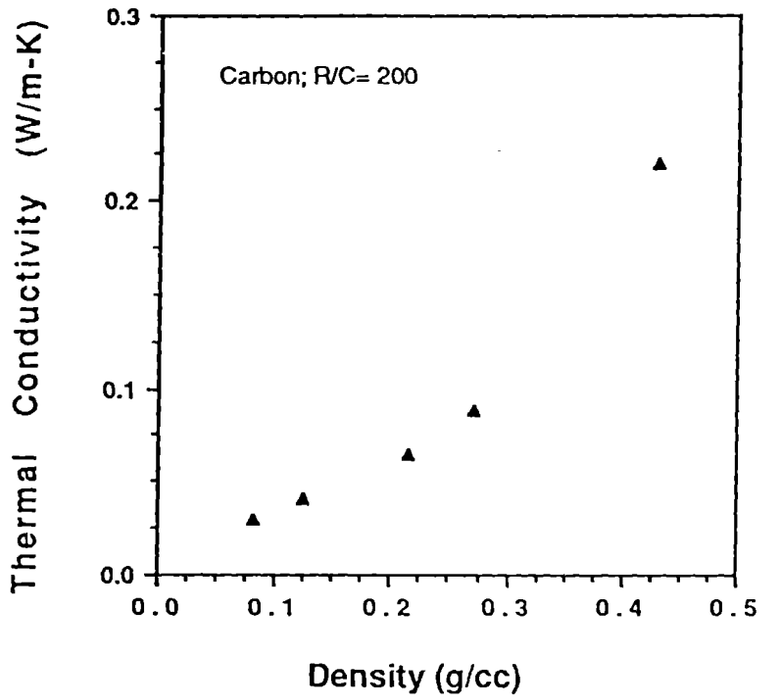
Carbon; R/C= 200
Thermal Conductivity (W/m-K)
0.3
0.2
0.1
0.0
0.0
0.1
0.2
0.3
0.4
0.5
Density (g/cc)

Fig. 5

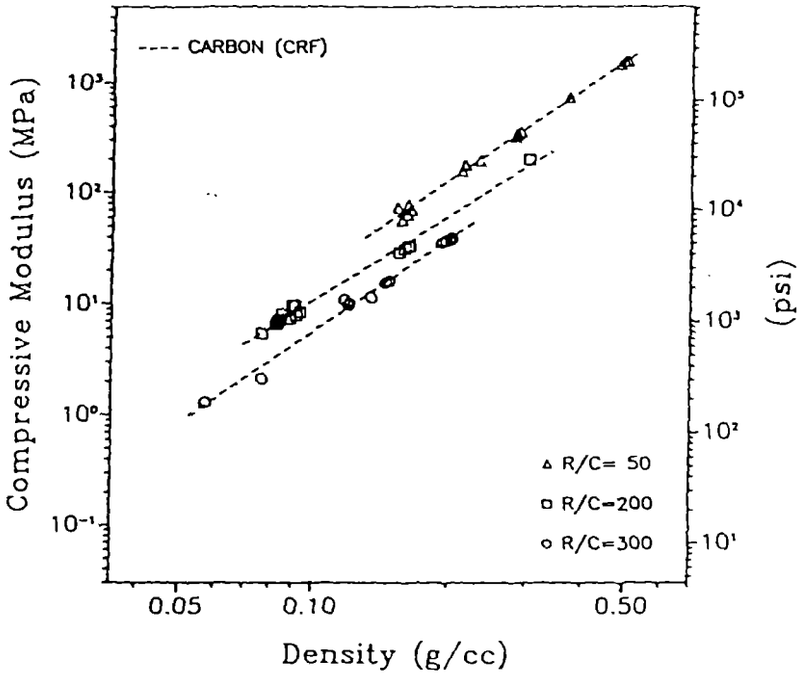
---- CARBON (CRF)
Compressive Modulus (MPa)
10^3
10^2
10^1
10^0
10^{-1}
10^5
10^4
10^3
10^2
10^1
(psi)
△ R/C= 50
□ R/C=200
○ R/C=300
0.05
0.10
0.50
Density (g/cc)

Fig. 6

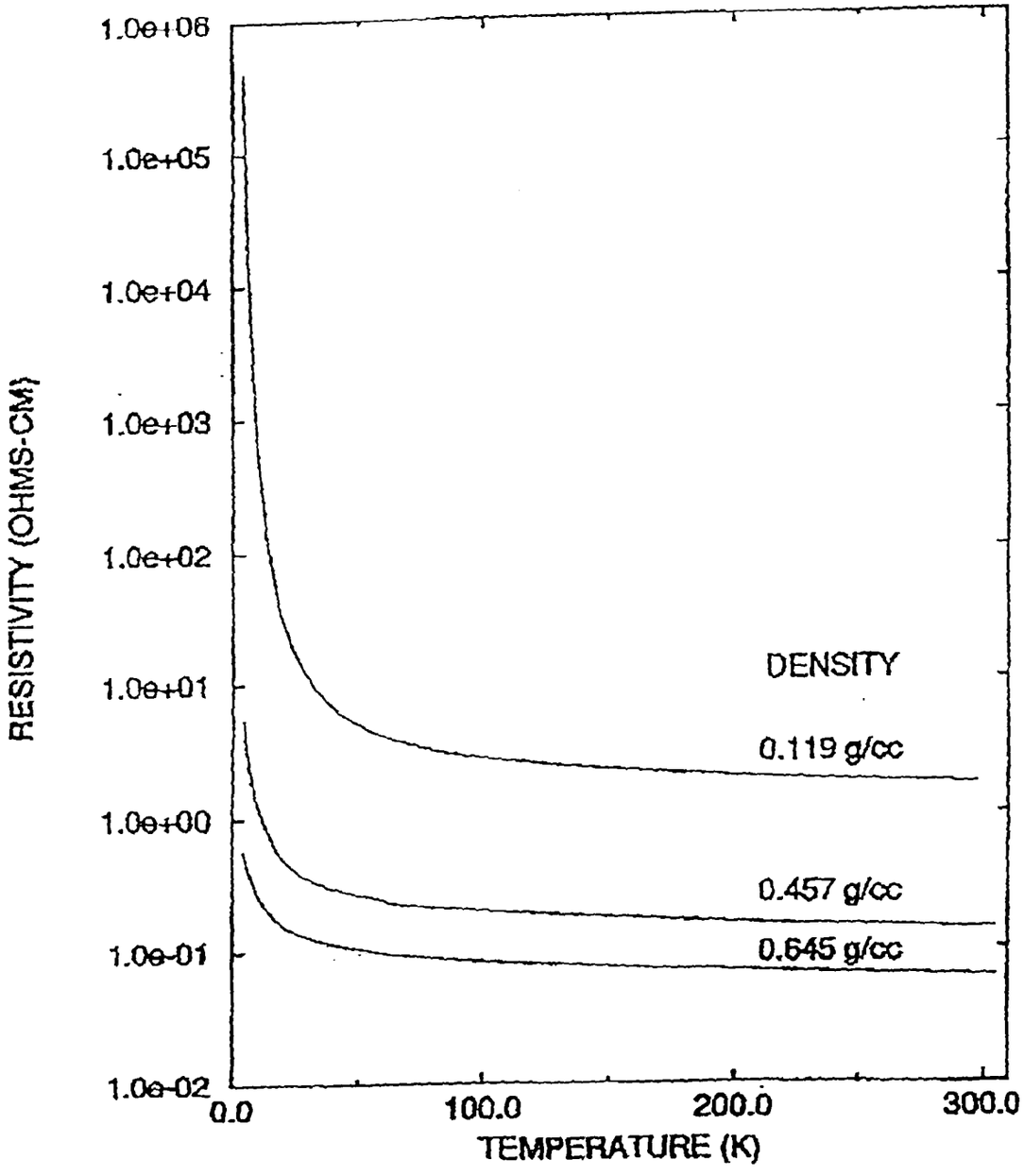
1.0e+06
1.0e+05
1.0e+04
1.0e+03
1.0e+02
1.0e+01
1.0e+00
1.0e-01
1.0e-02
RESISTIVITY (OHMS-CM)
DENSITY
0.119 g/cc
0.457 g/cc
0.645 g/cc
0.0
100.0
200.0
300.0
TEMPERATURE (K)

Fig. 7

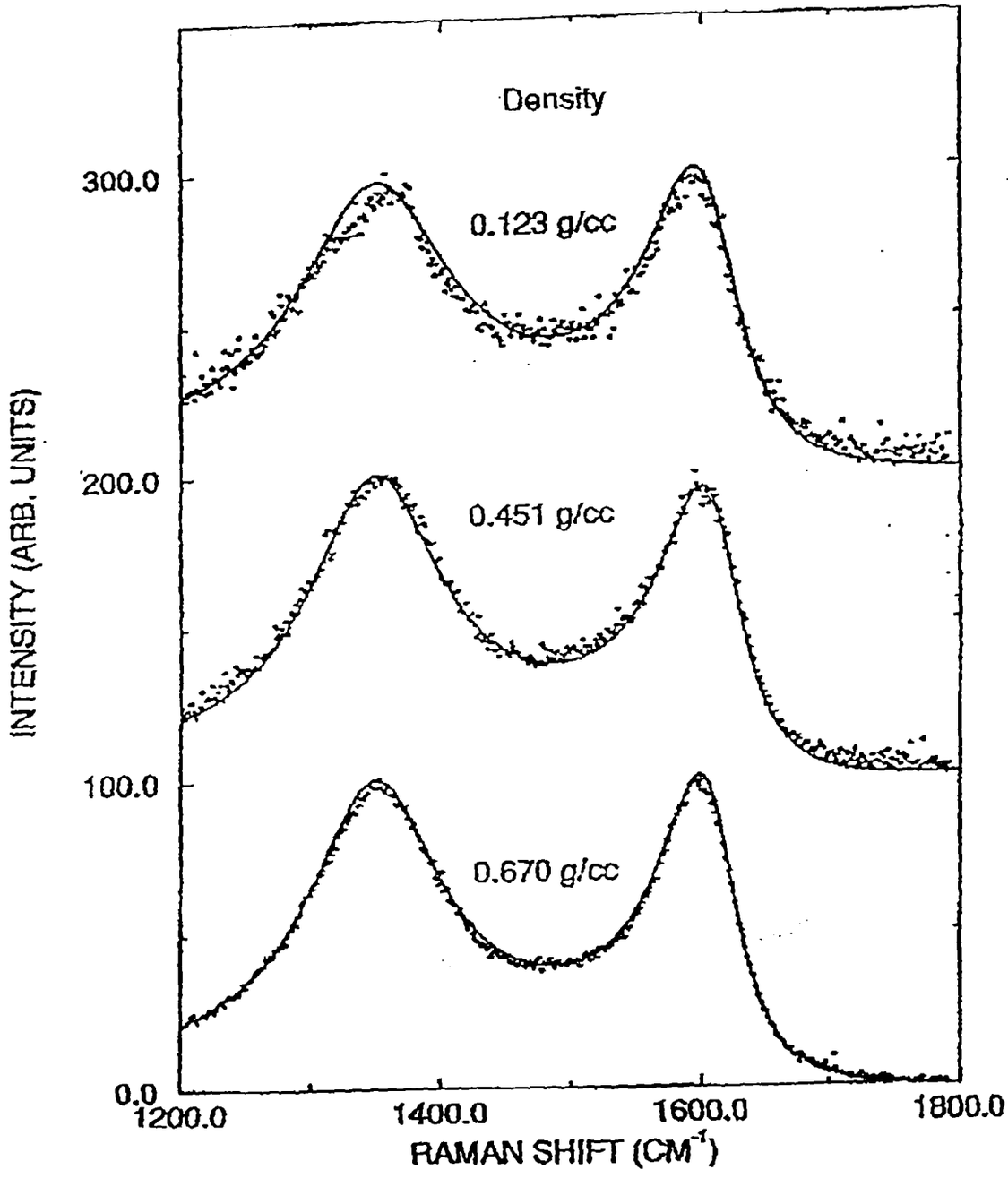
Density
0.123 g/cc
0.451 g/cc
0.670 g/cc
300.0
200.0
100.0
0.0
1200.0
1400.0
1600.0
1800.0
INTENSITY (ARB. UNITS)
RAMAN SHIFT (CM^{-1})

Fig. 8